Available online at www.sciencedirect.com
ScienceDirect
Journal of Power Sources 164 (2007) 697–703
JOURNAL OF POWER SOURCES
www.elsevier.com/locate/jpowsour

Reduced contact resistance of PEM fuel cell's bipolar plates via surface texturing

A. Kraytsberg, M. Auinat, Y. Ein-Eli *

Department of Materials Engineering, Technion-Israel Institute of Technology, Haifa 32000, Israel

Received 18 July 2006; received in revised form 5 November 2006; accepted 18 November 2006
Available online 3 January 2007

Abstract

Polymer electrolyte fuel cell performance strongly depends on properties of the stack bipolar plates. Stainless steel, being an attractive material for bipolar plates, raises major concern as having a high contact resistance. It is assumed that most of this contact resistance is governed by electrical properties of the developed oxide surface film. Accurate consideration of existing data and measurements of mechanically treated stainless steel/carbon interface reveals a substantial influence of surface topography on the contact resistance. Contact resistance may change tenfold, depending on substrate surface treatment and roughness. A model describing carbon/stainless steel interface is introduced, explaining the observed behavior.

Keywords: Contact resistance; PEM fuel cells; Bipolar plates; Mechanical texturing

1. Introduction

Polymer membrane electrolyte fuel cells (PEM FC) are a promising power source due to their high efficiency and near-zero emission. High cost, low power density and lifetime of fuel cell systems remains a major barrier to their wide use. A major influence on FC cost and power density is made by fuel cell stack bipolar plates, which connect electrically the adjacent cells of the stack and provide the gas supply to the cells. Currently, the most common bipolar plate material is graphite and its composite polymer materials. Whereas, graphite has a very good corrosion resistance and low electrical contact resistance with electrode gas diffusion layer materials, graphite is a costly material, and bipolar plate price makes up about 12% of total FC price. In addition, graphite is brittle and thus, highly difficult to be machined; It also does not offer enough high thermal conductivity. Due to its material properties, graphite bipolar plates need to have a thickness in the order of several millimeters, which makes a fuel cell stack heavy and voluminous: noticeably, graphite bipolar plates weight 88% of vehicle-size PEM FC [1].

The development of new materials for bipolar plates is crucial in order to increase specific power of PEM FC and lower PEM FC price. Alternative bipolar plate materials should fulfill the following requirements in order to be applicable: low-cost, easy to machine or to shape, lightweight and low volume, mechanically and sufficiently chemically stable, and having a low contact resistance. Price, availability, good manufacturability, high corrosion resistance and strength make stainless steel (either with or without a protective and conductive coating) a material of choice for bipolar plates.

At the same time, a point of concern is a high contact resistance of a stainless steel bipolar plate and a gas diffusion layer (which commonly, is based on carbon paper or carbon cloth) [2–4]. In a single PEM fuel cell, a polymer membrane is inserted between two gas diffusion layers coated with catalyst which is further sandwiched between two current collectors. Multiple fuel cells are stacked together in most practical applications to provide sufficiently high power and a desired voltage. The cells are separated by bipolar plates, which secure electron current flow all through the stack. This setup results in the amplification of the losses from contact resistance between contacting gas diffusion layers and bipolar plates, and as a result, this parameter has a dramatic effect on PEM FC stack efficiency and cost. Increase in contact resistance results in a power loss in the order of 2–5% per each additional 25 mV (per cm^2), if compared to

* Corresponding author. Tel.: +972 4 829 4588; fax: +972 4 829 5677.
E-mail address: eineli@tx.technion.ac.il (Y. Ein-Eli).

0378-7753/$ – see front matter © 2006 Elsevier B.V. All rights reserved.
doi:10.1016/j.jpowsour.2006.11.033

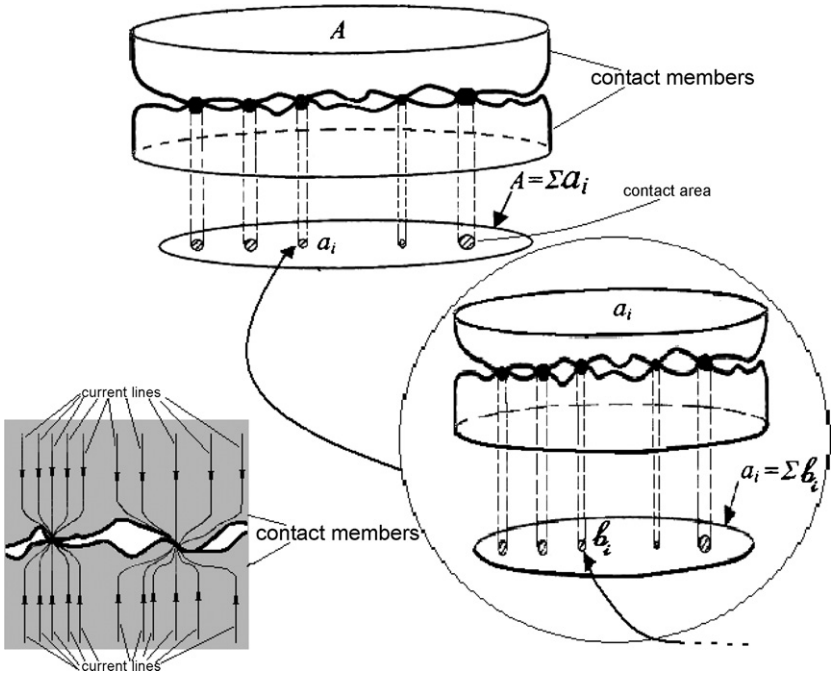

Fig. 1. Schematic of real contact spots in case of normal contact surfaces (top and right) and a current constriction (left).

graphite [5], while the price of a PEM FC stack (per kW) is estimated to be three times higher if the stack resistance increases from 0.05 Ω cm^{-2} to 0.2 Ω cm^{-2} [6]. The performance of a PEM FC system can be significantly improved if the contact losses can be minimized.

It is the formation of passive layers on the surface of stainless steels, which secures corrosion resistance of these materials. It is commonly accepted that this oxide layer (which appears on stainless steel bipolar plate in a highly acidic PEM FC environment) is responsible for the contact resistance on an interface of a stainless steel bipolar plate and gas diffusion layer [4,7–9]. Nevertheless, the experimental data on this matter are not in a good agreement with this concept. On the one hand, direct measurements of conductivity of a passive film, which appears on different stainless steel samples, in course of their electrochemical testing, provide far higher values than the values, which are generally observed in working fuel cell conditions [7]. On the other hand, not all the data on contact resistance developed so far can provide explanation on the substantial surface conductivity degradation of different stainless steels observed in a PEM FC environment [10,11].

2. Theory of contact resistance

To bring all these findings in line with one another, due attention should be given to the microscopic topography of a bipolar plate–gas diffusion layer interface. As of now, it is commonly accepted that contact resistance is governed by the surface topography of the contacting pair: the roughness features at the contacting surfaces decrease the actual area in contact and current flows only through the contact asperities, which is leading to a voltage drop across the interface, as shown in Fig. 1.

There are two limiting cases: one is a classical case, which is applicable when a contact size is much larger than the mean free path of electrons. It is so-called Holm contact resistance which is expressed in Eq. (1) [12]:

$$R_{\mathrm{H}} = \frac{\rho}{2r} \tag{1}$$

Here ρ is the bulk resistance (both contacting members are of similar material) and r is the contact radius of a circular contact. By now, there are many detailed considerations, which deal with contacts of different shapes and different surface concentration of the contact asperities [13]. Nevertheless, in all these cases, the general type of relation between contact resistance, R_{contact}, and contact size, r, is similar to Eq. (1): $R_{\mathrm{contact}} \sim r^{-1}$.

The other case is a quantum case, which is valid for the opposite limit, i.e., the contact size is much smaller than the mean free path of electrons (l_{e}) in the material; it is so-called Sharvin resistance, expressed in Eq. (2) [14]:

$$R_{\mathrm{Sh}} = \frac{4\rho l_{\mathrm{e}}}{3\pi r^2} \tag{2}$$

Here l_{e} is the mean free path of electrons. Eq. (3), below, represents the general case, for any contact size r or more specifically, for any ratio of l_{e}/r:

$$R = \frac{4\rho l_{\mathrm{e}}}{3\pi r^2} + \nu(l_{\mathrm{e}}/r)\frac{\rho}{2r} \tag{3}$$

Here $\nu(x)$ is a slowly varying function of the Knudsen ratio $K = l_{\mathrm{e}}/r$, which is represented in Fig. 2 [15].

Earlier models typically assumed the sizes of the actual contact asperities from experimental or theoretical points and then, assuming the asperities being enough widely spaced to be treated as resistances in parallel within a “macroscopic contact area”.

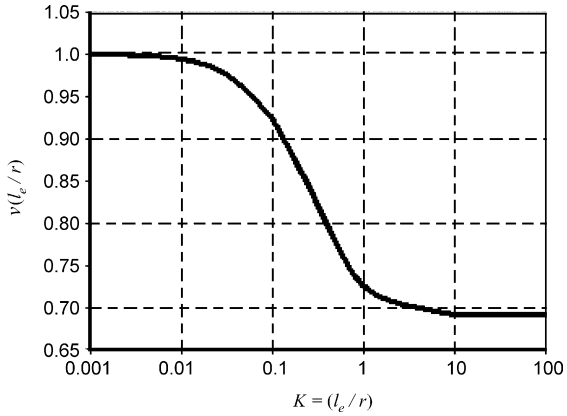

Fig. 2. Interpolation function $\nu(x)$ *vs.* Knudsen ratio $K = l_e/r$ [15].

Advances in surface measurement show that roughness is a multi-scale phenomenon; it was developed that a single contact appearing on one scale may be resolved as a cluster of smaller contacts on the next smaller scale (see Fig. 1). Though the advanced contact resistance models are using such considerably sophisticated fractal geometry related concepts as fractal roughness and fractal dimension [16], this does not change the proposition that contact resistance originates from current constriction in contact asperities and depends on the topography of the surfaces of the contacting members.

It is intuitively clear that if contact members are pressed one toward another, the contact resistance drops as pressure increases. First of all, the effect takes place because of the increase in contact area under the load: each contact spot increases the area because of material deformation and the amount of contacting spots increases because of dropping of contacting member separation. These conclusions are fully supported by detailed mathematical considerations [16]; the theory predicts a steep exponential-type contact resistance increase with the pressure drop as illustrated in Fig. 3.

There is little detailed information in the literature concerning surface topography of metal bipolar plates, and theirs related contact resistance. To gain better understanding of the influence of this parameter on the contact resistance of bipolar plates in a practical fuel cell conditions, we report here on studies performed on stainless steel and a carbon paper contact resistance with different surface roughness.

3. Experimental

Samples were cut out from a 0.4 cm thick ANSI 316 L sheet; one side of the sample was hand-grinded using grit no. 500 SiC-based emery paper. Other side of each sample (studied surface) was hand-grinded with a set of SiC-based emery papers: from 127 μm down to 1 μm-size grain diamond polishing paste and then washed with ethanol in ultrasonic bath. The resulting surface was profiled using atomic force microscope (AFM, Picoscan MI) and the resistance of the samples in contact with TORAY paper (TOR7-134J, 7 mils = 178 μm thick) was measured. No data from the vendor (TORAY) regarding bulk resistance under pressure was given. TORAY disc (Ø1 cm)

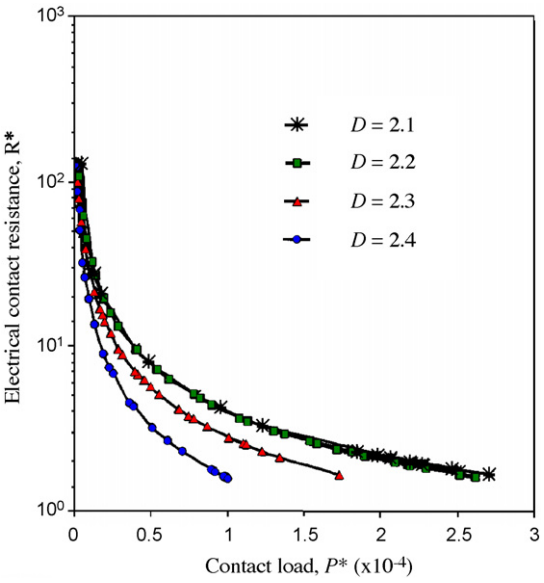

Fig. 3. Dimensionless electrical contact resistance R^* *vs.* dimensionless contact load P^* for contacting rough surfaces with the ratio of elastic modulus (E) to yield strength (Y), $E/Y = 106$, mean free path of electrons $\lambda^* = 0.03$, fractal roughness (root mean square deviation of the height differences along a given baseline) $G^* = 10^{-7}$ and various values of fractal dimension D ($D = 2.1$, 2.2, 2.3 and 2.4; A value of $D = 2$ represents an absolutely smooth surface which grows up when roughness is introduced) [16].

was pressed against the sample surface by an upper anvil (copper rod, Ø1 cm) with a preset pressure of 200 psi (1.4×10^6 N m^{-2}). The anvils' surfaces were machined and carefully hand-grinded (using grit no. 500 SiC-based emery paper) before each set of measurements. Constant current of a preset value I was applied to the sample and a voltage drop ΔV_{anvil} between upper and lower anvils was measured. The resistance R_{anvil} was determined as a slope of ΔV_{anvil} (I) line. The contact resistance values measured between copper and Toray, and respectively between copper and steel are similar. It is important to note that the measurement equipment is limited, once considering very small resistance. Practically, a measured potential value of ±0.5 mV can be measured; when a resistance of 2×10^{-3} Ω at 1 A cm^{-2}, is considered, we can (in reality) obtain 2.5×10^{-3} Ω in one case (say, in case of copper–Toray) and 1.5×10^{-3} Ω in another case (say, in case of copper–steel). Apparently, the error turns to be negligible (about 2%) even in case of the least measured resistance (22×10^{-3} Ω).

4. Results and discussion

The voltage drop ΔV_{anvil} and the resistance R_{anvil} follows Eqs. (4.0) and (4.1):

$$\Delta V_{\text{anvil}} = \Delta V_{\text{anvil}}^{\text{low}} + \Delta V_{\text{anvil}}^{\text{up}} + \Delta V_{\text{ss}} + \Delta V_{\text{Toray}} + \Delta V_{\text{ss-Cu}} + \Delta V_{\text{Cu-T}} + \Delta V_{\text{ss-T}} \quad (4.0)$$

$$R_{\text{anvil}} = R_{\text{anvil}}^{\text{low}} + R_{\text{anvil}}^{\text{up}} + R_{\text{ss}} + R_{\text{Toray}} + R_{\text{ss-Cu}} + R_{\text{Cu-T}} + R_{\text{ss-T}} \quad (4.1)$$

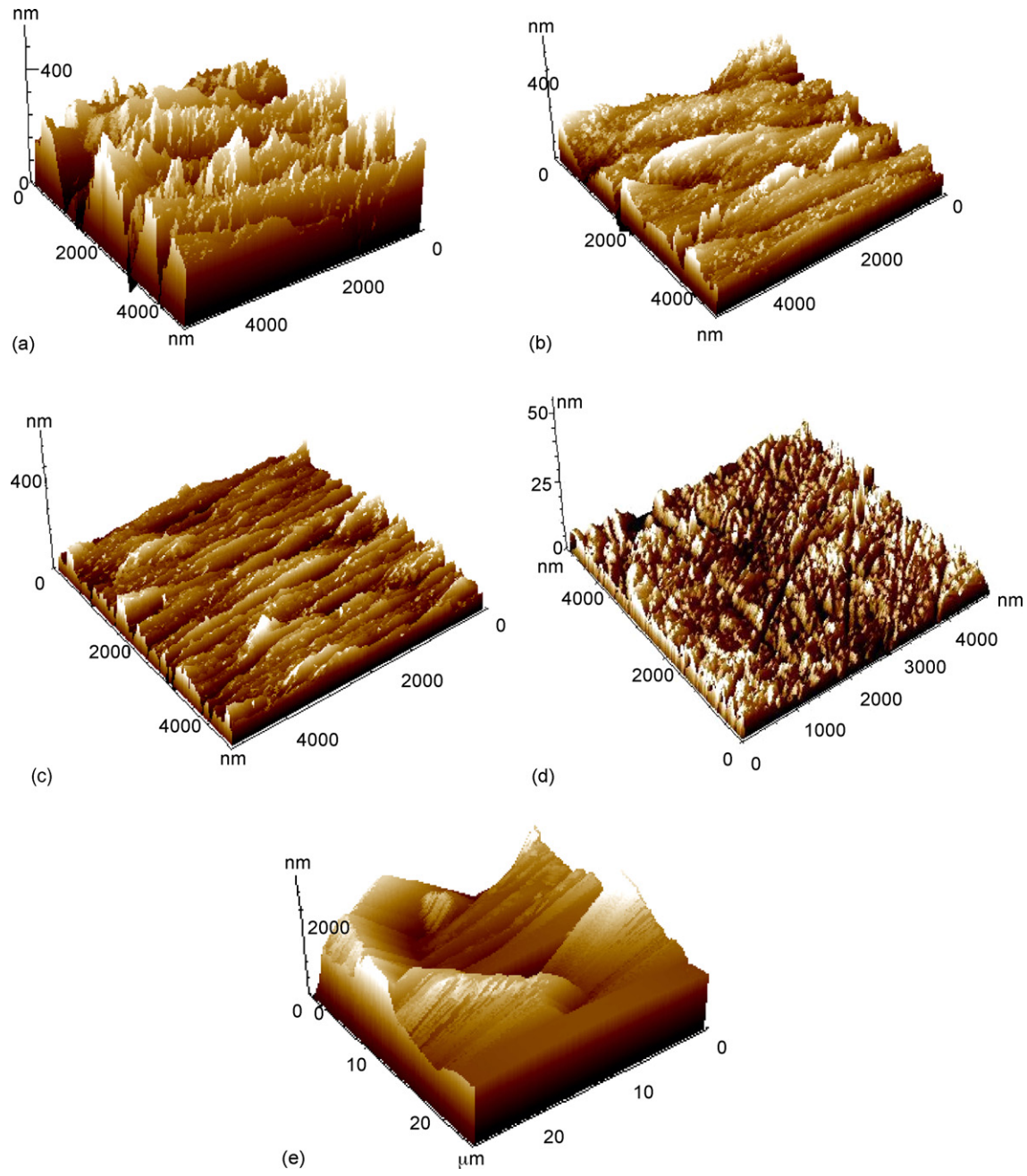

Fig. 4. 3D atomic force microscope (AFM) images of ASTM316L stainless steel surfaces treated with (a) 127 μm-emery paper; (b) 8 μm-emery paper; (c) 6.5 μm-emery paper; (d) 1 μm-diamond powder; (e) TORAY paper surface image.

Table 1
Emery paper treatment of ANSI 316 L stainless steel: surface roughness *vs.* grit size

	Grit size (μm)								
	127	53	36	30	16	8	6.5	1[a]	Toray
Contact resistance (mΩ)	22	28	36	29	23	86	100	361	NA
Average ridge height (nm)	188	101	90	60	27	15	9	10	8000

[a] Polished with 1 μm diamond powder.

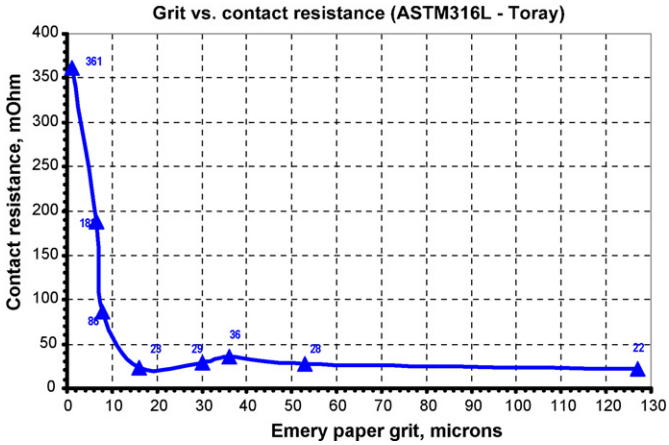

Fig. 5. Surface roughness *vs*. contact resistance values obtained from ASTM316L stainless steel surfaces (treated with different grades of emery paper) in contact with TORAY paper.

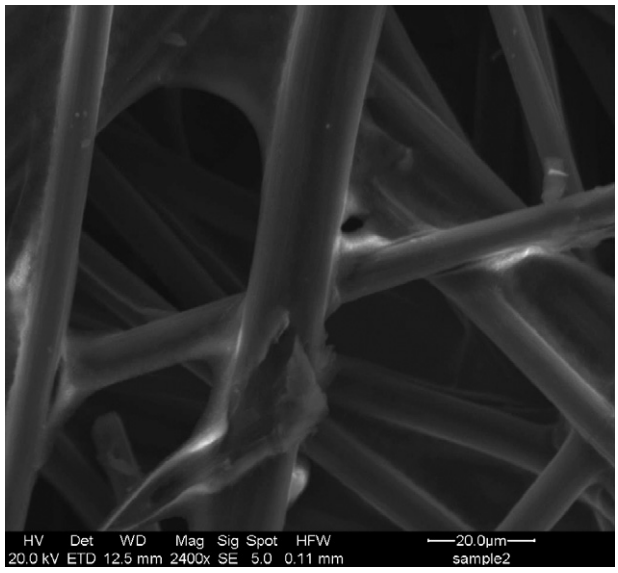

Fig. 6. Scanning electron microscope (SEM) image of the TORAY paper.

Here $\Delta V_{\text{anvil}}^{\text{low}}$ ($R_{\text{anvil}}^{\text{low}}$) is a voltage drop (and respectively resistance) across the lower copper anvil, $\Delta V_{\text{anvil}}^{\text{up}}$ ($R_{\text{anvil}}^{\text{up}}$) is a voltage drop (and respectively resistance) across the upper copper anvil, ΔV_{ss} (R_{ss}) is a voltage drop (and respectively resistance) across the sample body, ΔV_{Toray} (R_{Toray}) is a voltage drop (and respectively resistance) across the Toray disc, $\Delta V_{\text{ss-Cu}}$ ($R_{\text{ss-Cu}}$) is a voltage drop (and respectively resistance) across the back side of stainless steel sample–copper anvil interface, $\Delta V_{\text{Cu-T}}$ ($R_{\text{Cu-T}}$) is a voltage drop (and respectively resistance) across the copper anvil–Toray disc interface, and finally $\Delta V_{\text{ss-T}}$ ($R_{\text{ss-T}}$) is a voltage drop (and respectively resistance) across the stain-

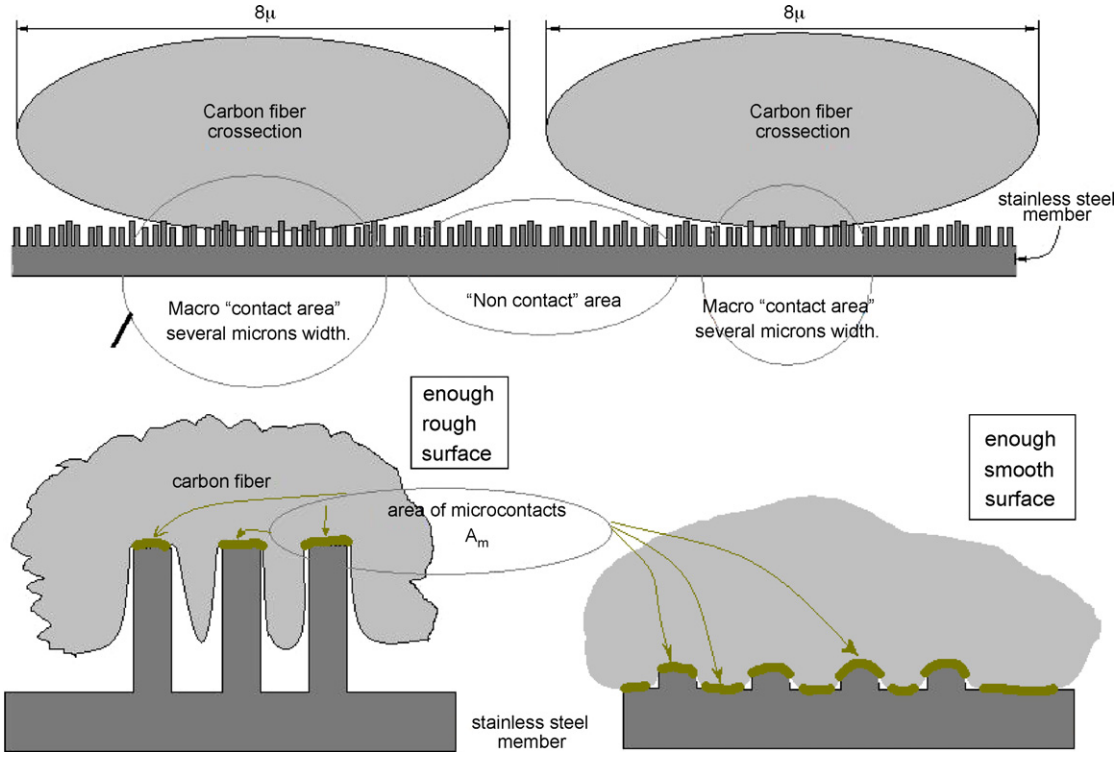

Fig. 7. Schematic representation of carbon paper/stainless steel contact area. Enough rough surface (of the most rigid member of the contact) is defined as a surface with micro-relief (micro-bumps, micro-ridges), which character height (the height of the most numerous ridges) is substantially bigger then the deformation of the other (soft) member of the contact. Vice versa, enough smooth surface (of the most rigid member of the contact) is the surface with micro-relief (micro-bumps, micro-ridges), which character height (the height of the most numerous ridges) is of the same order of magnitude as the deformation of the other (soft) member of the contact. This definition depends on the pressure and stiffness of the soft member. Surface, which is enough rough at some pressure values, may turn to be smooth enough under elevated pressure.

less steel sample test surface and Toray disc surface contact. The values of $\Delta V_{\text{anvil}}^{\text{low}}$ ($R_{\text{anvil}}^{\text{low}}$) ($10^{-6}\,\Omega$ and voltage drop less then 1.3×10^{-6} V in the whole current range), $\Delta V_{\text{anvil}}^{\text{up}}$ ($R_{\text{anvil}}^{\text{up}}$) ($10^{-5}\,\Omega$ and voltage drop less then 1.3×10^{-5} V in the whole current range) and, ΔV_{ss} (R_{ss}) ($1.5 \times 10^{-5}\,\Omega$ and voltage drop less then 2×10^{-5} V in the whole current range) were calculated using specific resistance values of the materials and were found negligible. R_{Toray} was calculated according to the vendor specification and found to be $1.8 \times 10^{-3}\,\Omega$; this value was taken in consideration. The $\Delta V_{\text{Cu-T}}$ ($R_{\text{Cu-T}}$) was determined by placing a Toray paper shim directly between upper and lower anvils. The value was found to be $2.0 \times 10^{-3}\,\Omega$; this value also was taken in consideration. The $\Delta V_{\text{ss-Cu}}$ ($R_{\text{ss-Cu}}$) was determined by placing a stainless steel sample with both surfaces hand-grinded with grit no. 500 SiC-based emery paper. The value was found to be $2.0 \times 10^{-3}\,\Omega$; this value also was taken in consideration.

Typical 3D relief of emery paper grinded ANSI316 steel samples is presented in Fig. 4a–d. Fig. 4e present an AFM image obtained from a TORAY paper, as well. The obtained set of AFM imaging points on a considerably anisotropic nature of the surface, with high "ridges" and deep "valleys" along the direction of hand-grinding movement. The tops of the ridges are considerably rough, whereas the bottoms of the valleys are comparatively smooth; a detailed data concerning the relief profile across ridges and along valleys are presented in Table 1.

Fig. 5 demonstrates that the contact resistance is nearly independent of the surface roughness down to the samples grinded with 16 μm emery paper. The samples, which has smoother surface (treated with 8, 6.5 μm emery paper and with 1 μm diamond powder), have a substantially higher contact resistance.

Carbon paper comprises of carbon fibers (Fig. 6), which are approximately 8 μm in diameter. The fibers have high anisotropic mechanical properties; their elastic modulus and yield strength values are far lower than the parameters measured for stainless steel [17]. Taking into consideration the fiber size and the characteristic dimensions of stainless steel relief, the contact area might be schematically represented as shown in Fig. 7.

It may be assumed that the spots of mechanical and electrical contact are presented only in "micro-contact areas", or areas of actual contact, A_{m}. This area size may be roughly estimated as the average ridges, which are detectable by AFM and whose average size is represented in Table 1. It may be assumed that when the surface becomes smoother (ridges smaller), the actual contact areas, A_{m}, increase in size. This increase results in diminishing of an actual pressure, (because the load, which is being applied in consideration to maintain the same force per unit of a sample apparent area, is unchanged) in the areas of actual contact A_{m}. The decrease of the pressure is proportional to the increase of the area of A_{m} whereas, the dependence of contact resistance *versus* pressure has nonlinear and very steep character (see Fig. 3); as a result, the decrease of the specific contact conductivity cannot be compensated by increasing in the contact area and the overall resistance is expected to grow up as can be seen exactly in Fig. 5.

5. Conclusions

The presented data demonstrate the substantial impact of the metal's surface relief, which contacts a carbon fiber-made material, onto contact resistance of metal/carbon material interface. Contrary common beliefs flattening the metal surface may results in a steep drop of the contact conductivity. It is essential to choose a proper mechanical treatment (and hence a proper surface topography) of bipolar plates to achieve a high value of bipolar plates/gas diffusion layers conductivity. The optimal parameters of the BPP surface relief are to be chosen in consistency with geometrical structure of the gas diffusion layer and mechanical properties of chosen carbon fibers, which constitute the gas diffusion layer. It should be stressed that no general bipolar plates/gas diffusion layer interface model concerning the most appropriate texturing (in terms of contact resisitivity) of the bipolar plates can be drawn from this study, since different gas diffusion layers may be applied in different fuel cell design. It may be suggested that the choice of suitable protective (anti-corrosion and conductive) plating cannot be adequately made without proper monitoring of the BPP surface topography.

References

[1] A.S. Woodman, E.B. Anderson, K.D. Jayne, M.C. Kimble, Development of Corrosion-Resistant Coatings for Fuel Cell Bipolar Plates, in: American Electroplaters and Surface Finishers Society, AESF SUR/FIN '99 Proceedings, 1999, 6/21-24.
[2] J. Wind, R. Spah, W. Kaiser, G. Bohm, Metallic bipolar plates for PEM fuel cells, J. Power Sources 105 (2002) 256–260.
[3] D.R. Hodson, et al., New lightweight plate system for polymer electrolyte membrane fuel cells, J. Power Sources 96 (2001) 233–235.
[4] Jinping Zhang et al., United States Patent 6,878,478.
[5] R.C. Makkus, A.H.H. Janssen, F.A. de Bruijn, R.K.A.M. Mallant, Use of stainless steel for cost competitive bipolar plates in the SPFC, J. Power Sources 86 (2000) 274–282.
[6] E.J. Carlson, P. Kopf, J. Sinha, S. Sriramulu, Y. Yang, Cost Analysis of PEM Fuel Cell Systems for Transportation, *TIAX LLC Cambridge, Massachusetts,* Subcontract Report, NREL/SR-560-39104, December 2005. http://www.tiaxllc.com/aboutus/pdfs/nrel_fnlrpt_093005.pdf.
[7] J.S. Kim, W.H.A. Peelen, K. Hemmes, R.C. Makkus, Effect of alloying elements on the contact resistance and the passivation behavior of stainless steels, Corros. Sci. 44 (2002) 635–655.
[8] A.K. Iversen, Stainless steels in bipolar plates—surface resistive properties of corrosion resistant steel grades during current loads, Corros. Sci. 48 (2006) 1036–1058.
[9] R.F. Silva, D. Franchi, A. Leone, L. Pilloni, A. Masci, A. Pozio, Surface conductivity and stability of metallic bipolar plate materials for polymer electrolyte fuel cells, Electrochim. Acta 51 (2006) 3592–3598.
[10] D.P. Davies, et al., Stainless steel as a bipolar plate material for solid polymer fuel cells, J. Power Sources 86 (2000) 237–242.
[11] D.P. Davis, et al., Bipolar plate materials for solid polymer fuel cells, J. Appl. Electrochem. 30 (2000) 101–105.
[12] R. Holm, Electric Contacts Handbook, Springer-Verlag, Berlin, 1958.
[13] R.S. Timsit, Electrical contact resistance: properties of stationary interfaces, IEEE Trans. Comp. Packaging Tech. 22 (1) (1999) 85–98.

[14] Y.V. Sharvin, Sov. Phys. JETP 21 (1965) 655–662.
[15] Sumit Majumder, et al., Study of contacts in an electrostatically actuated micro-switch, Sens. Actuators A 93 (2001) 19–26.
[16] L. Kogut, K. Komvopoulos, Electrical contact resistance theory for conductive rough surfaces, J. Appl. Phys. 94 (2003) 3153–3162.
[17] N.C. Gallego, D.D. Edie, Structure–property relationship for high thermal conductivity carbon fibers, Comp. Part A 32 (2001) 1031–1038.